Frequency metrology on the Mg 3s(2) S-1 -> 3s4p P-1 line for comparison with quasar data

Hannemann, S.; Salumbides, E.J.; Witte, S.; Zinkstok, R.T.; van Duijn, E.J.; Eikema, K.S.E.; Ubachs, W.M.G.

published in
Physical Review A. Atomic, Molecular and Optical Physics
2006

DOI (link to publisher)
10.1103/PhysRevA.74.012505

document version
Publisher's PDF, also known as Version of record

Frequency metrology on the Mg $3s^2\ ^1S \rightarrow 3s4p\ ^1P$ line for comparison with quasar data

S. Hannemann, E. J. Salumbides, S. Witte, R. Th. Zinkstok, E.-J. van Duijn, K. S. E. Eikema, and W. Ubachs
Laser Centre, Department of Physics and Astronomy, Vrije Universiteit, De Boelelaan 1081, 1081 HV Amsterdam, The Netherlands
(Received 12 May 2006; published 14 July 2006)

We report a frequency metrology study on the Mg $3s^2\ ^1S \rightarrow 3s4p\ ^1P$ transition near 202.5 nm. For this purpose, the fourth harmonic of the output from an injection-seeded Ti:sapphire pulsed laser is employed in a Mg atomic beam experiment with laser-induced fluorescence detection. Absolute frequency calibration with a frequency comb laser is performed on the cw seeding radiation, while the chirp-induced frequency shift between the pulsed output and the seed light is monitored on line. The resulting transition frequency for the main isotope ^{24}Mg is determined at 49 346.756 809(35) m^{-1}. This value is three orders of magnitude more precise than the best value in the literature. The line positions of the other isotopes ^{25}Mg and ^{26}Mg are also measured at comparable accuracy, giving rise to very exact values for the isotopic shifts. The achieved precision for the transition frequency at the 7×10^{-10} level makes this second resonance line of Mg I an additional candidate for inclusion in many-multiplet methods, aimed at detecting a possible temporal variation of the fine-structure constant α from comparison with quasar spectra. The isotopic shifts obtained are also important to correct for possible systematic shifts due to evolution of isotopic abundances, which may mimic α-variation effects.

DOI: 10.1103/PhysRevA.74.012505 PACS number(s): 32.30.−r, 42.62.Fi, 39.30.+w, 98.62.Ra

I. INTRODUCTION

The recent findings [1] claiming a possible variation of the fine-structure constant $\alpha=e^2/4\pi\epsilon_0\hbar c$ touch upon the very foundations of physics. A recent analysis by Murphy *et al.* [2] combining data from 128 quasar absorption systems over redshift ranges of $0.2<z_{abs}<3.7$ shows $\Delta\alpha/\alpha=(-0.543\pm0.116)\times10^{-5}$, a result at the 5σ confidence level. Notwithstanding the detailed data reduction and error analysis [3] the findings of this group, using the Keck telescope for observations of quasars in the northern hemisphere, are disputed by other groups, using the Very Large Telescope of the European Southern Observatory, monitoring quasar absorption systems in the southern hemisphere. [4,5]

The method used to extract information on a possible variation of α, the many-multiplet (MM) method [6,7], includes a number of atomic (and ionic) fine-structure splittings in a comparison between quasar and zero-redshift absorption features. The method requires extensive first-principles atomic-structure calculations of relativistic corrections to level energies, resulting in characteristic q factors for each atomic transition that represent the sensitivity for a certain spectral line to depend on a variation of α. The q factors for a number of atomic and ionic spectral lines including magnesium have been calculated [8]. For the transition frequencies at $z=0$ the most accurate literature values are used in the comparisons, but for many lines the uncertainties in the laboratory spectra are equally large as, or even larger than, those of the quasar features. Recently Berengut *et al.* [9] have produced a list of lines that could be implemented in the MM method to improve constraints on variation of α, if improved laboratory data became available. The $3s^2\ ^1S \rightarrow 3s4p\ ^1P$ transition in Mg I was identified as one that needed a more accurate rest-frame frequency determination.

In addition, because isotope abundances in the early universe and at distant locations in space may differ from those on Earth, accurate measurements of isotope shifts are required to quantify systematic effects and to prevent varying isotope abundances from mimicking variations of α. In particular, for magnesium, contributing several lines to the MM methods with large isotopic shifts, there exists an ongoing dispute on the isotopic evolution of the abundance ratio and its consequences for variations of α [10–12]. For these reasons a renewed interest has arisen in the determination of isotope shifts through refined *ab initio* calculations [13,14].

In view of the need for improved spectral data, we have reinvestigated the Mg I $3s^2\ ^1S \rightarrow 3s4p\ ^1P$ spectral line near 202 nm. The most accurate determination of the transition frequency for this second resonance line in the singlet system of magnesium dates back to the classical study of Risberg [15]. While the $3s^2\ ^1S \rightarrow 3s3p\ ^1P$ first resonance line has been the subject of many high-resolution investigations, focusing on the absolute transition frequency [16,17], the isotope shift [18–20], and even the hyperfine structure of ^{25}Mg [21], such detailed studies have not been performed for the $4p$ level.

In the present experimental investigation, a pulsed laser source, tunable near 202 nm, is used for exciting the $3s^2\ ^1S \rightarrow 3s4p\ ^1P$ in Mg. This approach, with the unavoidable intrinsic broadening due to the pulse structure of the light source, is chosen because of the difficulty in producing radiation in the deep-uv via nonlinear conversion with continuous-wave lasers. Using a pulsed titanium:sapphire (Ti:Sa) oscillator in the near-infrared range, three stages of nonlinear conversion are required to attain deep-uv wavelengths [22]. The frequency metrology using a home-built frequency comb laser setup [23,24] is performed on the output of the continuous-wave (cw) laser, which also seeds the oscillator cavity of the pulsed laser system. As is known from pulsed-dye laser systems, frequency excursions during the temporal pulse evolution (known as frequency chirp) may cause a net shift between the center frequency of the pulse and the cw frequency seeding the pulsed amplifier [25–27]. For the calibration of the singlet $3s4p$ level in Mg

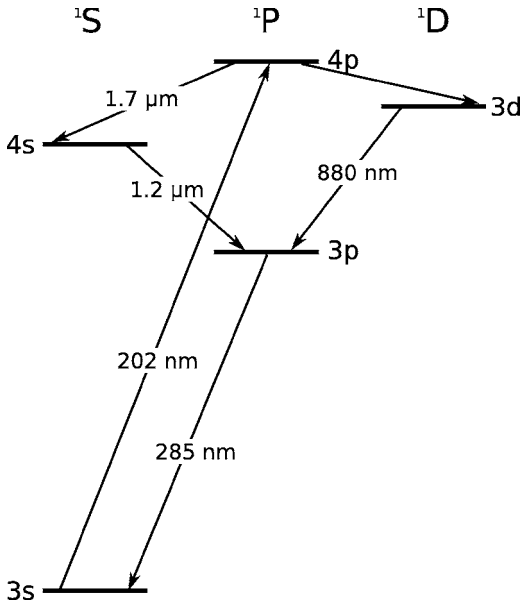

FIG. 1. Term level scheme of the singlet system of Mg showing the excitation and decay channels of the $3s4p\ ^1P$ level investigated. The laser excitation is at 202 nm and the 285 nm fluorescence from the $3s3p$ to the ground state is monitored in the experiment.

we have performed extensive measurements on these chirp effects, which are a limiting factor on the attainable accuracy in the transition frequency.

II. EXPERIMENTAL SETUP AND PROCEDURES

A. Mg atomic beam setup

Figure 1 depicts the term levels of the singlet system in Mg that are relevant for the excitation and detection scheme used in the present study. The excited $3s4p$ state has a lifetime of 14 ns [28] and decays back to the ground state via three channels. While the resonant decay has a branching ratio [29] of ≈85%, both of the remaining two channels—2% via $3s4s$, 13% via $3s3d$—decay to the $3s3p$ level that eventually emits 285 nm light upon relaxation to the ground state. This allows for off-resonant fluorescence detection at 285 nm with the advantage of efficient filtering of the 202 nm background with a Schott UG5 color filter.

A schematic of the atomic beam apparatus including the laser excitation and laser-induced fluorescence (LIF) detection zone is shown in Fig. 2. Metallic magnesium is heated in an oven to about 700 K producing an effusive atomic beam that is collimated downstream by two skimmers (S1, 0.5 mm diameter, and S2, 2 mm diameter) to reduce the transverse velocity spread. The line broadening due to the transverse velocity spread of the skimmed atomic beam is about 20 MHz.

Any deviation from the perpendicular alignment of the atomic and laser beams will result in a Doppler shift. To address this issue, the laser beam is split into two paths and then aligned such that the laser beams are counterpropagating collinearly as they cross the atomic beam. As long as the two laser beams are exactly counterpropagating, the first-order Doppler shifts in both beams will be of opposite signs and the unshifted line position can be obtained by taking the average of the line positions resulting from either laser path. The burden of establishing perpendicular atomic and laser beam alignment is then transposed to ensuring that the counterpropagating laser beams are perfectly aligned. However, it should be noted that the laser beams are aligned preferably perpendicularly to the atomic beam in order to achieve maximum signal-to-noise ratio.

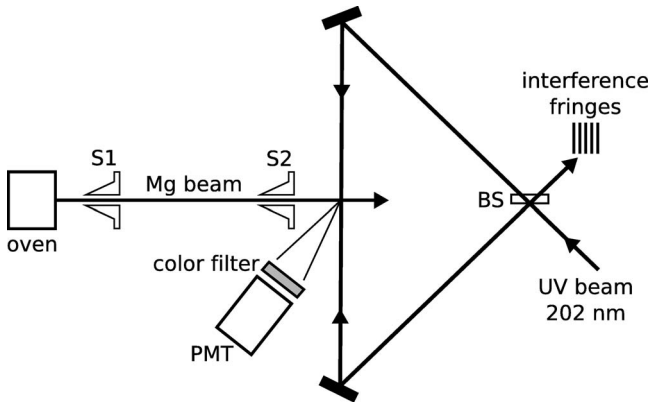

FIG. 2. Experimental arrangement of the off-resonance laser-induced fluorescence detection using a collimated Mg atomic beam. The excitation laser beam is split and the two paths are aligned to be perfectly counterpropagating, making use of the Sagnac-interferometer configuration. S1 and S2, skimmers; BS, beam splitter; PMT, photomultiplier tube.

An interferometric alignment technique is employed in order to align the counterpropagating beams to less than $\delta = 0.1$ mrad misalignment, which corresponds to a Doppler shift of about 350 kHz in the deep uv. As shown in Fig. 2, the excitation laser beam is split into two paths and then recombined to form a Sagnac interferometer. Special care was taken to ensure that the distances between beam splitter and interaction region are equally long for both light branches and that the two arms are of comparable intensity. Moreover the light is collimated with a beam diameter of about 1 mm at the interaction region. The advantage of the Sagnac setup is its robustness against acoustic disturbances which modulate the arm length of the interferometer. Since those disturbances affect both counterpropagating light beams in the same way, the path difference and likewise the interference pattern remain unchanged. In fact the interference pattern is predominantly influenced by the angle δ between the two contributing arms. When δ is lowered to zero the interference will show a dark fringe, which is especially useful as a sensitive alignment technique. In a two-beam interference pattern the relation between fringe periodic distance L and the angular misalignment θ of the two interfering beams is given by

$$\frac{\lambda}{L} = \sin\theta \approx \theta = 2\delta. \tag{1}$$

Geometric consideration shows that an angular mismatch δ between the counterpropagating beams within the Sagnac interferometer will lead to an angle $\theta = 2\delta$ on the screen. The

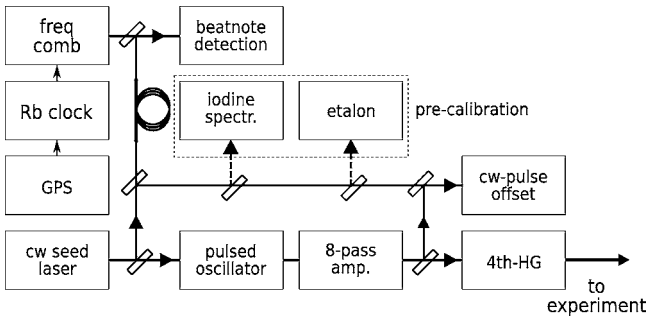

FIG. 3. Schematic representation of the experiment. The amplified output of a Ti:Sa pulsed oscillator is upconverted to the fourth harmonic, and the resulting 202.5 nm light is used in the atomic beam setup as depicted in Fig. 2. The cw pulse frequency offset is monitored throughout the measurement. The frequency of the cw Ti:Sa seed radiation is measured with a femtosecond frequency comb, which is referenced to a Rb frequency standard with global positioning system (GPS) time correction. A precalibration with an I_2 saturation setup is performed to determine the correct mode of the frequency comb.

attainable accuracy for the angular alignment is restricted by the beam diameter, because it determines the spot size on the screen and likewise the maximum resolvable fringe period L. Identifying the fringe period L with the beam diameter $d=1$ mm yields the aforementioned possible misalignment of $\delta=0.1$ mrad. Since the interferometer alignment does not drift from dark fringe to the first-order fringe pattern showing up on the screen the accuracy for δ is actually better. Still we keep this uncertainty level as a conservative measure. A more detailed discussion of the interferometric alignment to eliminate first-order Doppler shifts will be provided in a forthcoming presentation.

B. The deep-uv laser source

A schematic representation of the laser system and frequency metrology setup is shown in Fig. 3. The uv laser source has been described in some detail before [22]. The system consists of a Ti:Sa pulsed oscillator that is injection seeded with light from a cw Ti:Sa ring laser and is actively locked using the Hänsch-Couillaud (HC) scheme. The pulsed oscillator produces Fourier-limited pulses of 20 MHz linewidth centered at the cw seed wavelength of about 810 nm, with a typical pulse energy of 0.1 mJ. The pulses are subsequently sent through an eight-pass amplification stage to enhance the pulse energy to about 8 mJ. In order to produce the fourth harmonic at 202.5 nm, three consecutive nonlinear upconversion stages—BBO crystals cut at appropriate type-I phase matching angles—are used [22]. The resulting radiation near 202.5 nm has a repetition rate of 10 Hz, bandwidth 40 MHz, and a typical pulse length of about 15 ns. The pulse energy of the excitation laser beam can be chosen by varying the pump power sent to the multipass amplifier. The laser system reaches maximum output energies of 0.2 mJ/pulse at the fourth harmonic. However, in order to reduce saturation effects we usually work with pulse energies of not more than 0.1 μJ which corresponds to an intensity of about 1 kW/cm^2 at the interaction zone. Using those settings typically observed linewidths were about 50 MHz, which corresponds to the width one expects when convoluting the laser linewidth, the residual Doppler broadening and the natural linewidth of the $3s^2\ ^1S \rightarrow 3s4p\ ^1P$ transition.

Since the absolute frequency calibration is performed on the cw Ti:Sa seeding radiation, it is necessary to assess the possible frequency difference between the pulsed output and the injected seeding light. Such frequency offsets might be caused by frequency excursions during the temporal pulse evolution (chirp) due to the intensity-dependent refraction index of the lasing medium [25–27] and by dynamical mode-pulling effects in the pulsed oscillator resonator. In order to address both effects, we followed strategies recently explored by White *et al.* [30,31] for determining chirp phenomena in an injection-seeded and pulsed optical parametric oscillator. A more extensive description of the cw pulse frequency offset characterization will be given in a forthcoming presentation [32].

It is possible to adjust the cw pulse offset and set it close to zero by changing parameters of the pulsed oscillator HC lock. The frequency chirp is minimized by lowering the pump power to the pulsed oscillator. Typically, the cw pulse frequency offset is centered around zero and has a standard deviation of less than 0.5 MHz, for the entire duration of the measurement. During the spectroscopic scans a multitude of data from each single pulse is registered. We use a single oscilloscope to measure the LIF signal, the uv power, and the net cw pulsed frequency difference from each laser pulse acquired. This correlated acquisition technique allows for data filtering in the analysis procedure. Thus it is possible to use the power fluctuations of the uv-laser output, simply by taking many data points during one scan. The acquired data are subsequently binned with respect to the uv pulse intensity. By this means possible excitation-intensity-dependent line shifts can be assessed during the scans.

C. Absolute calibration procedures

The absolute calibration is performed on the cw seeding light from the Ti:Sa ring laser. Part of the cw seed light is coupled through a 100 m single-mode optical fiber toward the laboratory where a frequency comb reference laser [24] is located. The cw light is heterodyned with the output of this frequency comb and the radio-frequency beat note is detected in a spectrometer setup using an avalanche photodiode. Typically, the beat-note detection reached a signal-to-noise ratio of 45 db. The two main parameters of the frequency comb are its carrier-envelope phase offset frequency ν_{CEO} and its repetition rate ν_{rep}. Both are locked to a rubidium-clock standard, which is further referenced to the synchronization signal of the global positioning system. From the locking characteristics, and from the fact that a scan over one isotopic line takes about two minutes we estimate the precision of the calibration with the frequency comb to be better than 25 kHz—which corresponds to an accuracy of less than 100 kHz in the deep uv.

An absolute calibration with a frequency comb requires the frequency to be known in advance within a fraction of

the frequency spacing of neighboring modes in the comb, which is equal to the repetition rate of the laser ($\nu_{\mathrm{rep}} \approx 75$ MHz). Since the $3s^2\ ^1S \rightarrow 3s4p\ ^1P$ transition frequency is only known [15] within 0.07 cm^{-1}, a precalibration procedure is required. For that purpose, part of the cw seeding light is used to perform iodine saturation spectroscopy in a setup developed by the Knöckel *et al.* [33] specially suited for the near-infrared wavelength region. It consists of an iodine cell which is heated to about 900 K in order to populate high rovibrational levels in the $X\ ^1\Sigma_g^+$ ground state of I_2. For reducing the pressure in the cell, it has a cold finger extension which is temperature stabilized at room temperature. After the precalibration the transition frequency of the $\mathrm{Mg}3s^2\ ^1S \rightarrow 3s4p\ ^1P$ line is known to a 10 MHz level of accuracy, which is sufficient for the final calibration using the frequency comb.

D. Measurement procedures

Since the frequency comb laser is situated in a different laboratory, the data acquisition and scan control software is divided onto two separate PCs which are linked via TCP/IP on a 100 Mbit/s ethernet connection. The system will be described in a forthcoming presentation in detail [32]. In short, the PC in the spectroscopy laboratory runs the actual laser scan and acquires and stores all retrieved data. On each scan step it sends a beat-note count request to the PC that controls the frequency comb, and receives the essential data from the frequency comb: the repetition rate ν_{rep}, the carrier envelope offset frequency ν_{CEO}, and the measured beat-note frequency ν_{bn} between the frequency comb and cw seed light.

The experimental procedure is as follows. The seed laser is tuned stepwise in frequency with an external control voltage provided by an arbitrary wave-form generator (Agilent AWG 33250A). Each scan is about 200 MHz wide (in the deep uv) and consists of about 300 equidistant voltage steps. While the cw-laser frequency is scanned the beat note between frequency comb and cw light changes likewise. In order to keep the beat-note frequency within a range of 21.7 ± 2 MHz—which is the working range of a frequency bandpass filter in the electronic beat-note frequency counting circuitry—the repetition rate of the frequency comb is adjusted after each scan step, so that the frequency components of the comb spectrum follow the seed light scan [32]. At each scan step the acquisition software obtains the relative uv power, the cw pulse frequency offset, and the LIF signal of ten laser shots. At the same time the computer that controls the frequency comb counts the beat-note frequency ten times per scan step within time gates of 0.1 s for each individual count. From those ten frequency counts the average value is used for the calibration, while the standard deviation is a measure for the short-term frequency jitter of the seed laser, which is about 1 MHz.

III. RESULT

The Mg spectrum with the I_2 calibration line and the étalon markers is shown in Fig. 4. The spectrum obtained from

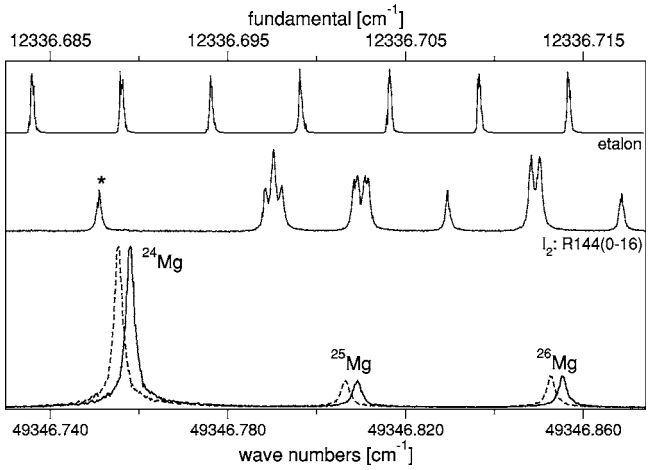

FIG. 4. The $3s^2\ ^1S \rightarrow 3s4p\ ^1P$ Mg spectrum showing the isotope splittings. A fraction of the seeding radiation at the fundamental wavelength is used to record the I_2 saturation signal and étalon markers (150 MHz FSR) for precalibration. The Mg spectrum obtained for the counterpropagating laser beam is drawn with a dashed curve. The *t* hyperfine component of the R144 line in the *B-X*(0 −16) band, predicted [33] at 12 336.687 74 cm^{-1}, is marked by an asterisk.

the counterpropagating beam is also indicated in the same figure. The angle between the light beam and the atomic beam was purposely misaligned from the near-perpendicular orientation to demonstrate the clear separation of the line centers obtained from each light beam path. For the subsequent calibrations using the frequency comb, the light beams were aligned back to the perpendicular setting. The positions of the hyperfine components of the I_2 R144(0-16) rovibrational line of the *B-X* transition used for the calibration were taken from the prediction software developed by Knöckel *et al.* [33]. The cw pulse offset was set to be around zero throughout the measurements.

First we performed calibration scans on the most abundant isotope ^{24}Mg. In order to obtain a Doppler-free frequency value for the $3s^2\ ^1S \rightarrow 3s4p\ ^1P$ transition, the Sagnac interferometer is first aligned until dark fringe is achieved. Then for each of the two light branches of the interferometer two scans are performed—one by tuning the laser from lower to higher frequencies and another scan with opposite tuning direction. For each of the four scans, a center line position is obtained by nonlinear least-squares fitting. Their arithmetic average gives the final transition frequency.

In order to check the reproducibility of the calibration the full procedure has been repeated five times. After each of the four-scan measurements not only was the Sagnac dark fringe realigned, but also the phase matching of the upconverting nonlinear crystals has been checked and optimized. Hence possible systematic frequency shifts, as a result of imperfectly aligned phase-matching angles or Sagnac dark fringe, acquire a statistical characteristic. Additionally, the relative uv excitation intensity has been changed by one order of magnitude, without showing any significant effect on the calibrated line position. In Table I the average value of the five calibrations is given. The contributions to the uncertainty budget are discussed below.

TABLE I. The line positions of the magnesium isotopes for the $3s^2\ ^1S \rightarrow 3s4p\ ^1P$ transition. The isotopic shifts obtained from the experiment are compared to *ab initio* calculations by Berengut *et al.* [14]. The given uncertainty intervals for the experimental values represent the final uncertainties as listed in Table II.

Isotope	Position (cm^{-1})	Shift from ^{24}Mg (MHz) expt.	Calc. [14]
^{24}Mg	49346.756809(35)		
^{25}Mg	49346.807724(40)	1526.4(1.2)	1530(50)
^{26}Mg	49346.854173(40)	2918.9(1.2)	2950(50)

For the ^{25}Mg and ^{26}Mg isotopes we performed two complete scan sets consisting of four scans each. The obtained frequencies are also given in Table I. Additionally, since the isotopic shifts can be obtained from relative measurements, after performing one complete scan set on ^{24}Mg the Sagnac interferometer was not realigned. Instead the seed laser was directly tuned to the other isotopic lines where spectroscopic scans were performed and frequency differences obtained by comparing the line positions taken from a single interferometer arm. The line positions for the less abundant isotopes given in Table I result from combined averaging of the two absolute calibrations and a number of relative measurements. The slightly larger uncertainties are due to the lower signal-to-noise ratio on the LIF signal of the weaker isotopes.

The scans on ^{25}Mg did not give significantly different measured linewidths compared to the even isotopes, which points to the fact that a possible hyperfine splitting on the odd isotope is very small. *Ab initio* calculations of the hyperfine constant A for the $3s4p\ ^1P$ state yields a value of $A = -3.3$ MHz,[1] which would lead to the hyperfine levels $\Delta E_{\mathrm{hfs}} = (-8.25, 3.3, 11.55)$ MHz for $F = (7/2, 5/2, 3/2)$. With an observed linewidth of 50 MHz for the main ^{24}Mg isotope—which is the convoluted linewidth of the instrumental width and the natural linewidth of the $3s^2\ ^1S \rightarrow 3s4p\ ^1P$ transition—it is impossible to resolve such a hyperfine structure, which is in agreement with the experiment.

In order to assess a possible line broadening for the observed ^{25}Mg line shape as a result of the calculated hyperfine splitting, we simulated a superposition of the three hyperfine lines using the observed linewidth of the ^{24}Mg isotope (see Fig. 5). In the upper part (a) of the figure, averaged data are shown as dots taken on the main ^{24}Mg and the ^{25}Mg isotope. Each dot represents an average of four pulses on the ^{24}Mg data and of seven pulses on the ^{25}Mg data. The solid curves depict fitted Lorentzian lines. The given linewidths in Fig. 5(a) represent average values taken from a multitude of spectroscopic scans. There is no significant difference in the observed line shapes of the ^{24}Mg and the ^{25}Mg isotopes as the small suggested difference can be explained by noise broadening—the observed linewidth of ^{26}Mg is 60(9) MHz. Figure 5(b) shows the three simulated hyperfine lines

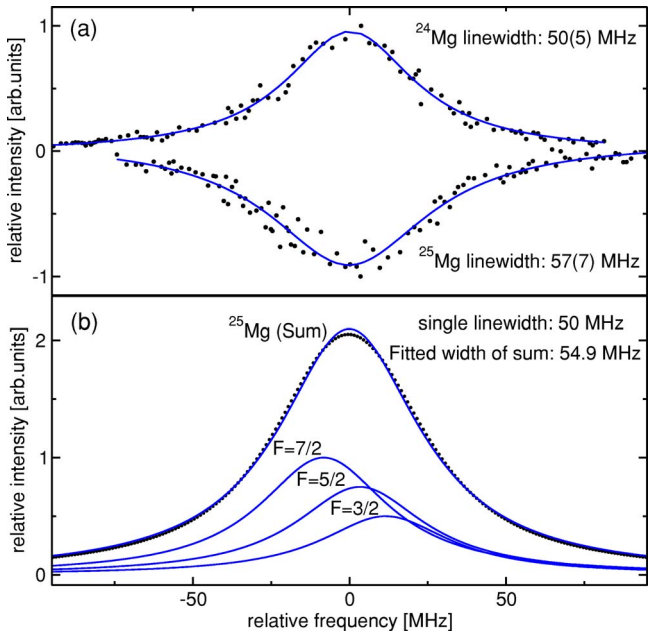

FIG. 5. (Color online) Comparison of the observed line shapes of the main ^{24}Mg isotope and the odd ^{25}Mg isotope (a). In the lower part (b) the three single hyperfine contributions with a linewidth as found on the main isotope (50 MHz) are separately depicted. The calculated sum of the three overlapping features is also shown as a dotted curve and a fit against the result is performed and depicted as solid line. Even though the hyperfine splitting between $F=7/2$ and $F=3/2$ is about 20 MHz, the linewidth of the sum is only marginally larger than a single peak linewidth.

(Lorentzian shape) which are intensity weighted by their multiplicities. The sum of the hyperfine lines is depicted as a dotted curve, which is fitted by another Lorentzian curve shown as solid line. Even though the hyperfine splitting between $F=7/2$ and 3/2 is about 20 MHz the resulting superposition gives only a small additional line broadening by about 5 MHz, which would not be visible in our experiment. It should be noted that the line center of the fitted curve in Fig. 5(b) is found exactly on the center of gravity of the simulated hyperfine structure. We conclude that the calculated hyperfine splitting constant $A=-3.3$ MHz fits well within our observed linewidth.

The contributions to the experimental error budget are listed in Table II. The table is split into two parts. Since the errors (i)–(iv) have statistical characteristics and are not related, a quadrature summation has been taken. It should be noted that error (iv) is only relevant for the isotopic shifts. The errors (v) and (vi) are of systematic character and estimated as maximum possible deviations. Error (vii) (second-order Doppler) is also systematic, but very small and can be neglected. For the total error budget the quatrature sum over errors (i)–(iv) has been added to the linear summation of errors (v) and (vi). It represents a final uncertainty for the resulting values for the absolute calibration and isotopic shifts.

As discussed earlier for the first-order Doppler error [position (i) in Table II] a conservative budget is given. In practice it turns out that the dark fringe alignment is quite stable

[1]These calculations were performed by L. Veseth (University of Oslo) and kindly made available to us.

TABLE II. Error budgets on the absolute calibration given in kilohertz at the deep-uv energy scale. The total confidence interval is obtained by taking the quadrature sum of the errors (i)–(vi) and linear summation of the result with the errors (v)–(vii). Errors (iii) and (iv) represent the 1σ uncertainties of the nonlinear least squares fit.

	Error	kHz
(i)	First-order Doppler	350
(ii)	Frequency comb	<100
(iii)	Fit error ^{24}Mg	200
(iv)	Fit error ^{25}Mg, ^{26}Mg	450
(v)	ac Stark	100
(vi)	cw pulse offset	500
(vii)	Second-order Doppler	8
	Total ^{24}Mg	1050
	Total ^{25}Mg,^{26}Mg	1200

and does not drift to a bright interference maximum during the measurements. Moreover, the persistent realignment of the Sagnac interferometer for each measurement procedure turns this possible systematic error into a statistical one, and can hence be reduced when taking more spectroscopic scans. The actual experimental spread (1σ) for the ^{24}Mg line-center frequencies is 510 kHz and about 600 kHz for the isotopic shifts, which is well below the given total error bars in Table II. The ac-Stark effect was too weak to be measured at the power levels used in a range 0.03–0.3 μJ/pulse. We estimate an upper limit to the ac-Stark shift based on the obtained statistics. For a more elaborate treatment of the cw pulse frequency deviations as a result of chirp, we refer to Hannemann *et al.* [32]. The frequency comb measurements result in line positions that are about 15 times more accurate compared to the I_2 precalibration procedure.

The final value for the transition frequency of the $3s^2\,{}^1S \rightarrow 3s4p\,{}^1P$ line entails an improvement of about three orders of magnitude from the results of classical spectroscopy by Risberg [15]. To our knowledge, the present experiment is the first to resolve the isotopic shifts for this transition. The precision of the isotopic shifts is comparable to those obtained by Hallstadius [18] for the $3s^2 \rightarrow 3s3p$ transition. We also tabulate the calculated isotopic shift using the parameters from Berengut *et al.* [14]. The comparison shows very good agreement between the experimental and the theoretical results.

It should be noted that the redshifted quasar absorption spectra do not resolve the isotopic structure of the $3s^2\,{}^1S \rightarrow 3s4p\,{}^1P$ line. Instead the resolution is given [2] as a full width at half maximum (FWHM) $\approx$6.6 km/s which corresponds to 33 GHz at 202 nm. Using our results and the natural isotopic abundancies on Earth as found by Rosman *et al.* [34]—^{24}Mg, 79.11(4)%, ^{25}Mg, 10.00(1)%, ^{26}Mg, 11.01(3)%—we simulated a merged line from the three isotopic lines each having a FWHM of 33 GHz and found the resulting line center at 49 346.772 52(7) cm^{-1}. This value, folded over the isotopic components, agrees within the 1σ uncertainty limit with the value reported by Risberg: 49 346.729(70) cm^{-1}. Recently, we learned about another spectroscopic study of the $3s^2\,{}^1S \rightarrow 3s4p\,{}^1P$ transition in Mg I. Aldenius *et al.* [35] measured 49 346.771(3) cm^{-1} based on Fourier-transform spectroscopy in which the isotopic components are not resolved. This value is a factor of 20 more accurate than the value of Risberg, and is in perfect agreement (within 1σ limits) with the present value of the folded line.

IV. CONCLUSION

We have performed an accurate determination of the $3s^2\,{}^1S \rightarrow 3s4p\,{}^1P$ transition frequencies of the three magnesium isotopes ^{24}Mg, ^{25}Mg, and ^{26}Mg. This investigation is motivated by current studies on the absorption spectra of extragalactic gas clouds at high redshift to probe a possible variation of the fine-structure constant α. With the frequency determination at the level of 7×10^{-10}, the Mg$3s^2\,{}^1S \rightarrow 3s4p\,{}^1P$ line may represent a welcome addition to the set of transitions used in the many-multiplet analysis in the search for a variation of α.

The isotope shift obtained at a 1 MHz accuracy should be helpful in assessing systematic effects that imitate an α variation due to the possible evolution of isotopic abundance [11]. For example, when taking the possible change in α as $\frac{\Delta\alpha}{\alpha}=(-0.543\pm0.116)\times10^{-5}$ from Kozlov *et al.* [11] and $q=87$ cm^{-1} for the $3s^2\,{}^1S \rightarrow 3s4p\,{}^1P$ transition in Mg as given by Berengut *et al.* [9], the transition frequency ν_{Mg} (unresolved for the isotopic contributions) should have been different by

$$\Delta\nu_{\mathrm{Mg}} = 2q\frac{\Delta\alpha}{\alpha} = -28.3(6.1)\ \mathrm{MHz} \qquad (2)$$

10^{10} years ago. With the isotopic shift obtained from this experiment a comparable change in ν_{Mg} could be mimicked by a 1% different abundance of ^{24}Mg in the isotopic composition of the magnesium used in the laboratory and existing at the point in space-time where the quasar absorption spectra were imprinted.

In addition, the values of the isotopic shifts for this transition are found to be in good agreement with the *ab initio* calculations of Berengut *et al.* [14]. It is reassuring that the theoretical predictions are in such good agreement, since the sensitivity coefficients q for possible variations of α [7,8] are calculated within the same framework.

ACKNOWLEDGMENTS

The Netherlands Foundation for Fundamental Research on Matter (FOM) is gratefully acknowledged for financial support. We thank Dr. H. Knöckel (Hannover) for providing us with the I_2 cell for near-ir saturation spectroscopy, Dr. L. Veseth (Oslo) for calculating the hyperfine constant in ^{25}Mg, Dr. J. Berengut (Sydney) for valuable discussions, and Dr. M. T. Murphy (Cambridge) for sending us a manuscript on recent Fourier-transform measurements prior to publication.

[1] J. K. Webb, V. V. Flambaum, C. W. Churchill, M. J. Drinkwater, and J. D. Barrow, Phys. Rev. Lett. **82**, 884 (1999).
[2] M. T. Murphy, J. K. Webb, and V. V. Flambaum, Mon. Not. R. Astron. Soc. **345**, 609 (2003).
[3] M. T. Murphy, J. K. Webb, V. V. Flambaum, V. A. Dzuba, C. W. Churchill, J. X. Prochaska, J. D. Barrow, and A. M. Wolfe, Mon. Not. R. Astron. Soc. **327**, 1208 (2001).
[4] R. Srianand, H. Chand, P. Petitjean, and B. Aracil, Phys. Rev. Lett. **92**, 121302 (2004).
[5] R. Quast, D. Reimers, and S. A. Levashkov, Astron. Astrophys. **415**, L7 (2004).
[6] M. T. Murphy, J. K. Webb, V. V. Flambaum, J. X. Prochaska, and A. M. Wolfe, Mon. Not. R. Astron. Soc. **327**, 1237 (2001).
[7] V. A. Dzuba, V. V. Flambaum, and J. K. Webb, Phys. Rev. Lett. **82**, 888 (1999).
[8] V. A. Dzuba, V. V. Flambaum, and J. K. Webb, Phys. Rev. A **59**, 230 (1999).
[9] J. C. Berengut, V. A. Dzuba, V. V. Flambaum, M. V. Marchenko, and J. K. Webb, e-print physics/0408017.
[10] T. Ashenfelter, G. J. Mathews, and K. A. Olive, Phys. Rev. Lett. **92**, 041102 (2004).
[11] M. G. Kozlov, V. A. Korol, J. C. Berengut, V. A. Dzuba, and V. V. Flambaum, Phys. Rev. A **70**, 062108 (2004).
[12] Y. Fenner, M. T. Murphy, and B. K. Gibson, Mon. Not. R. Astron. Soc. **358**, 468 (2005).
[13] J. C. Berengut, V. A. Dzuba, V. V. Flambaum, and M. G. Kozlov, Phys. Rev. A **69**, 044102 (2004).
[14] J. C. Berengut, V. V. Flambaum, and M. G. Kozlov, Phys. Rev. A **72**, 044501 (2005).
[15] G. Risberg, Ark. Fys. **28**, 381 (1965).
[16] N. Beverini, E. Maccioni, D. Pereira, F. Strumia, G. Vissani, and Y. Z. Wang, Opt. Commun. **77**, 299 (1990).
[17] J. C. Pickering, A. P. Thorne, and J. K. Webb, Mon. Not. R. Astron. Soc. **300**, 131 (1998).
[18] L. Hallstadius, Z. Phys. A **291**, 203 (1979).
[19] S. Le Boiteux, A. Klein, J. R. Rios, and M. Ducloy, J. Phys. (France) **49**, 885 (1988).
[20] A. Amy-Klein, O. Gorceix, S. Le Boiteux, J. R. Rios Leite, and M. Ducloy, Opt. Commun. **90**, 265 (1992).
[21] H. J. Kluge and H. Sauter, Z. Phys. **270**, 295 (1974).
[22] M. Sneep, S. Hannemann, E.-J. van Duijn, and W. Ubachs, Opt. Lett. **29**, 1378 (2004).
[23] S. Witte, R. Th. Zinkstok, W. Hogervorst, and K. S. E. Eikema, Appl. Phys. B: Lasers Opt. **78**, 5 (2004).
[24] S. Witte, R. T. Zinkstok, W. Ubachs, W. Hogervorst, and K. S. E. Eikema, Science **307**, 400 (2005).
[25] M. S. Fee, K. Danzmann, and S. Chu, Phys. Rev. A **45**, 4911 (1992).
[26] N. Melikechi, S. Gangopadhyay, and E. E. Eyler, J. Opt. Soc. Am. B **11**, 2402 (1994).
[27] K. S. E. Eikema, W. Ubachs, W. Vassen, and W. Hogervorst, Phys. Rev. A **55**, 1866 (1997).
[28] T. N. Chang, Phys. Rev. A **41**, 4922 (1990).
[29] J. Steiner and L. J. Curtis, J. Phys. B **37**, 3771 (2004).
[30] R. T. White, Y. He, B. J. Orr, M. Kono, and K. G. H. Baldwin, J. Opt. Soc. Am. B **21**, 1577 (2004).
[31] R. T. White, Y. He, B. J. Orr, M. Kono, and K. G. H. Baldwin, Opt. Lett. **28**, 1248 (2004).
[32] S. Hannemann, E. Salumbides, S. Witte, R. Th. Zinkstok, K. S. E. Eikema, and W. Ubachs (unpublished).
[33] H. Knöckel, B. Bodermann, and E. Tiemann, Eur. Phys. J. D **28**, 199 (2004).
[34] K. J. R. Rosman and P. D. Taylor, Pure Appl. Chem. **70**, 217 (1998).
[35] M. Aldenius, S. Johansson, and M. T. Murphy, Mon. Not. R. Astron. Soc. (to be published); e-print astro-ph/0605053,